Surface plasmon resonance from metallic columnar thin films

A. Shalabney [a], A. Lakhtakia [b,c], I. Abdulhalim [a,*], A. Lahav [a], Christian Patzig [d], I. Hazek [a], A. Karabchevsky [a], Bernd Rauschenbach [d], F. Zhang [b], J. Xu [b]

[a] *Department of Electrooptic Engineering, Ben Gurion University of the Negev, Beer Sheva 84105, Israel*
[b] *Department of Engineering Science and Mechanics, Pennsylvania State University, University Park, PA 16802-6812, USA*
[c] *Department of Physics, Indian Institute of Technology Kanpur, Kanpur 208016, India*
[d] *Leibniz-Institut für Oberflächenmodifizierung e.V., Permoserstrasse 15, 04318 Leipzig, Germany*

Abstract

Surface plasmon (SP) waves on the interface of a dielectric (such as water) and a metallic columnar thin film (CTF) of porosity as high as 0.55 were experimentally and theoretically investigated. The CTFs were made of Al, Au, Ag, or Cr. As the porosity increases, the SP resonance (SPR) dip was found to widen, shift to higher wave numbers, and become asymmetric due to increasing scattering losses. With further increase of porosity, the SPR dip was found to disappear, leaving behind only a peak near the onset to the total internal reflection regime. The shape of the nanoislands constituting the CTF is better described as ellipsoidal than as spherical or spheroidal, indicating thereby the existence of orientational biaxial anisotropy even for CTFs thinner than 60 nm. For a best fit between the theoretical calculations and the experimental data, the CTF was divided into two layers having different porosity and nanoisland shape, particularly for the Ag- and Au-CTFs. The sensitivity of the CTF-based SPR signal to refractive index variations of an analyte infiltrating the nanopores of and in the region adjoining the metallic CTF was found to be doubly enhanced compared to that for the SPR signal from a nonporous metallic film.

1. Introduction

Metallic nanostructured thin films are of immense interest these days [1] due to their widely increasing technological importance for applications such as solar-control mirrors, subwavelength optical imaging, and biosensing, partly due to the existence of the phenomenon of surface plasmon resonance (SPR) and its applicability for biosensing. SPR has been known for a long time [2] and is commonly used for sensing of chemicals [3]. In order to excite an SP wave, the tangential component of

the wave vector of the *p*-polarized incident light has to match the SP wave vector in magnitude. This match can be achieved using either a high-index prism at angles larger than the critical angle for total internal reflection (TIR) or a one-dimensional grating. A thin metal film is usually deposited on the prism or the grating and then *p*-polarized reflected light exhibits a sharp dip at the angle of incidence at which the component of the incident light's wave vector along the surface closely matches the wave number of the SP wave. This resonance occurs due to the real part of the relative permittivity of the metal being negative at optical frequencies.

A typical set-up for SPR sensors is the Kretschmann configuration, wherein one side of a high-index prism is

---

* Corresponding author.
 E-mail address: abdulhlm@bgu.ac.il (I. Abdulhalim).

coated with a thin metal film, typically Ag or Au. The metal plays two roles: first, excitation through the prism sets up evanescent fields that extend to the metal–sample interface; second, at that interface, SP waves can be excited when the tangential component of the wave vector of the incident light matches the SP wave vector in magnitude. The reflectance strongly decreases when the latter condition (called the SPR condition) is met due to absorption in the metal, and the width and the depth of the resonance are dependent on the type of the adjacent dielectric material. When the adjacent material is other than air, it is often referred to as the analyte, the term which we use here to include air as well. The described sensing method is sensitive to surface defects (due to oxidation of the metal film) and surface roughness, since the field strength is largest near the metal–analyte interface and the penetration depth in the analyte is rather small. Nonetheless, the width of the reflectance dip and the level of the reflectance minimum do yield information about the analyte, and the accuracy of the SPR sensor can be enhanced by optimizing the thickness of the metal film [4].

Surface plasmons can be localized on metallic nanoparticles and nanoshells [5,6]. Localized SPR (LSPR) can also arise at some locations either in or on certain porous or highly disordered materials [7]. The associated absorption resonances often show up in optical spectra as narrowband features. Spatial non-homogeneities can also lead to averages over many different localized resonances, the overall effect being broadened thereby.

In this paper, we investigate the SPR phenomenon on the surface of a nanoengineered columnar thin film (CTF) made of a metal. Sufficiently thick CTFs are assemblies of upright, parallel columns generally grown by physical vapor deposition (PVD) techniques [8]. Comprising clusters of 3–5 nm diameter, the columns can be considered as nanowires. CTFs can be made of inorganic and organic dielectric materials, polymers, metals, and semiconductors. For optical purposes, a CTF is a homogeneous continuum with anisotropic constitutive properties at visible and infrared wavelengths.

CTFs can be nanoengineered with non-homogeneity normal to the substrate plane and can be made of a variety of materials. A hallmark of a CTF is its porosity. Depending on the deposition conditions 10–300 nm void regions between the columns of similar cross-sectional dimensions can be achieved. It can be even more if the substrate is patterned with features that serve as seeds for the incoming particles flux. The porosity (voids volume fraction from the total volume) can be engineered from very low to very high values. Being

porous, a CTF can function as a nanoreactor. This capability can be harnessed for a variety of sensing applications. Very thin CTFs (<60 nm) may be considered as assemblies of tilted nanoislands.

Recently, LSPR was excited in porous metallic thin films – without prism coupling – due to scattering [9,10] and surface-enhanced phenomena such as Raman scattering [11–13] and fluorescence [14,15] were demonstrated. Extensive SPR experiments using prism coupling were performed in the past on films comprising metallic nanoislands [16,17] and long-range SPR [18] excitation was also demonstrated; however, those films were quite dense with porosity less than 0.2. In the majority of these experiments the theoretical fit to the experimental data was performed using the Maxwell Garnett effective medium formalism which works best when the porosity is either very low or very high. Otherwise, it is better to use the Bruggeman formalism set-up correctly for an anisotropic effective medium. [19,20]

We investigated the SPR phenomenon on the surfaces of porous metallic CTFs, using prism coupling in the visible regime. We also found that absorption in nonporous metallic films can produce a sharp and symmetric peak as the signature of the SPR phenomenon. Therefore the effect of two mechanisms of loss on the SPR was examined in thin metallic CTFs–absorption and scattering. Both mechanisms were found to cause broadening of the SPR dip remaining with a peak at the onset of TIR.

2. Experimental details

The CTFs chosen for this work were made of Al, Ag, Au or Cr. The CTFs made of Al were deposited in an electron-beam evaporation system (PVD-75, KJL Inc.). The oblique-angle-deposition technique was used, as depicted schematically in Fig. 1(a). With the vacuum base-pressure set below 4 μTorr in an evacuated chamber, collimated Al vapor was directed towards a 2.54 cm × 2.54 cm BK7-glass substrate at a fixed angle $\chi_v = 20°$ to the substrate plane. The distance between the Al source and the centroid of the substrate was fixed at 25.4 cm. The substrate was held stationary. The nominal deposition rate, monitored with a resonating quartz crystal sensor, was set to 0.25 nm/s. After deposition, a profilometer (Tencor P-10) was used to measure the metallic CTF's average thickness as 30 nm.

CTFs of Au and Ag were deposited on soda lime glass. Whereas the Au-CTFs were deposited with dc sputtering, the Ag-CTFs were deposited by means of electron-beam evaporation in a combined electron-
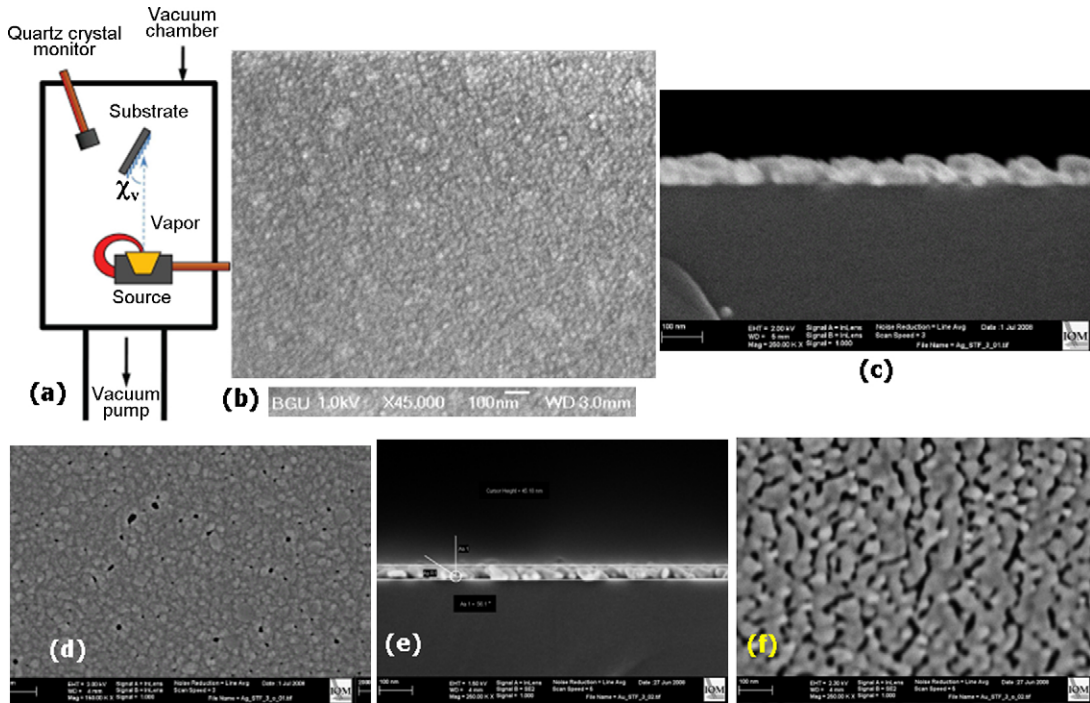
Fig. 1. (a) Schematic of the oblique-angle-deposition technique. Collimated vapor flux oriented at angle χ_v with respect to the substrate plane leads to the formation of parallel columns tilted at an angle $\chi \geq \chi_v$ to the same plane. (b)–(f) Typical scanning electron microscope images of CTFs made of (b) Al, (c) Ag (cross-section), (d) Ag (top view), (e) Au (cross-section), and (f) Au (top view). The scale bar in all images denotes 100 nm.

beam evaporation and sputtering system (Edwards). The distance between the source and the substrate was kept at approximately 12 cm for sputtering and 16 cm for electron-beam evaporation. The pressure while evaporating Ag was approximately 0.15 mTorr and while sputtering Au approximately 7.5 mTorr. The nominal deposition rates measured with a resonating quartz crystal sensor were held below 1 nm/s. The deposition flux was directed at angles fixed between 60° and 85° to the substrate normal (χ_v between 30° and 5°)

for different CTFs. The Cr films were prepared as dense films with vapor directed normally ($\chi_v = 90°$) to the substrate plane.

Table 1 summarizes the metallic CTFs used and their parameters. Fig. 1(b)–(f) is typical scanning electron microscope (SEM) micrographs showing the tilted columnar morphology of the CTFs we used. For reference measurements, dense films of Ag and Au were also prepared with vapor directed normally to the substrate plane.

Table 1
Parameters used for best fit between the theoretical simulations and the experimental data presented in Figs. 3 and 8. The parameters χ_j, d_j and p_j are the tilt angle of the nanowires with respect to the substrate plane, the thickness, and the porosity used for each of the two layers ($j = 1, 2$). The ellipsoidal shape factors of the jth layer are denoted by γ_{2j} and γ_{3j}.

| Sample	χ_1 (°)	χ_2 (°)	d_1 (nm)	d_2 (nm)	P_1	P_2	γ_{21}	γ_{31}	γ_{22}	γ_{32}
Al-CTF-1	70	70	30	0	0517	–	1.2	15	–	–
Al-CTF-2	70	70	30	0	0.6	–	1.2	15	–	–
Ag-CTF-2a	35	35	8	34	0.521	0.1	1.2	1.5	1	5
Ag-CTF-3a	85	90	16	24	0.09	0.08	1.16	1.2	1.2	2
Ag-CTF-4a	0	70	5	33	0.51	0.05	1.2	3.2	1.2	5
Au-CTF-3a	35	35	8	38	0.51	0.32	1	1	1.2	5
2nd fit	35	35	8	50	0.6	0.35	1	1	1	1
Au-CTF-4a	35	35	15	35	0.45	0.24	1	1	1.2	4
Au-CTF-5a	35	35	5	38	0.15	0	1	1	1.2	1.5
2nd fit	35	35	3.5	60	0.825	0	1	1	1.2	1.5
Au-CTF-6a	35	35	12	55	0.385	0.02	1	5	1.2	5
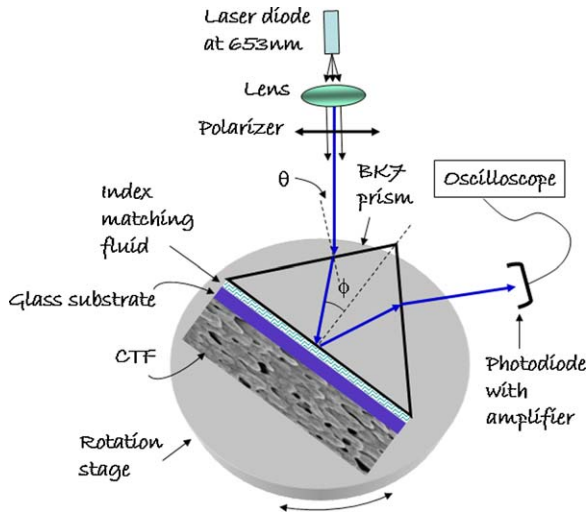
Fig. 2. Schematic of the Kretschmann configuration. The drawing is not to scale. The higher the value of the angle ϕ for SPR, the higher is the SP wave number.

The Kretschmann configuration of Fig. 2 was implemented with incident light coming from a 653 nm wavelength laser diode first collimated with a lens and then p-polarized after passage through a linear polarizer. The 45°–90°–45° prism used in the Kretschmann configuration was made of BK7-glass (refractive index = 1.51509). The glass substrate on which the metal CTF was deposited was separated from the prism by a thin layer of an index-matching fluid of index 1.52. The fraction R of the incident power density that exits the right slanted face of the prism was measured using an amplifying photodiode and an oscilloscope. The entire assembly was mounted on an optical table on which the angle of incidence θ on the prism can be set to 1°-precision. To ensure that the SPR phenomenon was correctly observed, the polarizer was rotated by 90° degrees to achieve the s-polarization state (instead of the p-polarization state), and it was verified that the SPR does not exist then.

3. Description of the numerical simulations

Numerical simulations of R as a function of θ were performed as follows: [21] The p-polarization transmittance T_{ag} across the air–glass interface on the left side of the prism was computed as a function of θ with the Fresnel formula, as also the p-polarization transmittance T_{ga} at the glass–air interface on the right side of the prism. The p-polarization reflectance R_{gca} of glass-CTF-sample at the base of the prism was computed as a function of the incidence angle θ, by using a simple matrix-based formalism wherein we

assumed that the nanowires of the CTF are tilted in the plane of Fig. 2 at an angle $\chi \geq \chi_v$, with respect to the substrate plane [8]. The reflectance R was estimated as the product $T_{ag}R_{gca}T_{ga}$, while the porosity p and layer thickness of the CTF were varied to fit the experimental data.

The effective relative permittivity tensor of the metallic CTF was obtained from a Bruggeman formalism [19,20,22], wherein it was assumed that the metal is distributed in the form of electrically small ellipsoids of aspect ratios 1:γ_2:γ_3, the void regions are electrically small spheres, the void regions are vacuous, the porosity p lies between 0 and 1. It should be mentioned that Yang et al. [18] used the Maxwell Garnett approach to perform their theoretical fit to experimental data. Furthermore, although Yang et al. [10] used the Bruggeman approach for the same purpose, they assumed that both the metal and air (void) are distributed as identical, electrically small, prolate spheroids because they took the effective medium to be uniaxial. Thus our Bruggeman approach is substantially different as it allows the effective medium to be biaxial. Moreover, while Yang et al. [10] treated the depolarization dyadic (of a prolate spheroid) as an unknown to which they fitted their experimental data, we assume that both shape factors γ_2 and γ_3 of ellipsoids are unknowns.

4. Results and discussion

4.1. Aluminum CTFs

The relative permittivity of bulk Al equals $-59.288 + 22.2385i$ at 653 nm wavelength. For simulating the SPR phenomenon with an Al CTF, we set the tilt angle $\chi = 70°$, CTF thickness as 30 nm, and the ellipsoids to be of aspect ratios 1:1.2:15. Fig. 3(a) shows the measured values of R versus the incidence angle θ, when the analyte is air. The sudden drop in R as θ changes from 5° to 0° indicates the excitation of an SPR. The wide dip in the R–θ curve is indicative of scattering loss due to the spatial non-homogeneity of matter in the CTF. Fitting the numerically simulated reflectance R as a function of the internal angle of incidence ϕ to the experimental data, we found that $p = 0.517$; i.e., the Al CTF is 51.7% volumetrically porous.

Next, we etched the Al CTF using the Transene [23] Al etchant of type A, for 5 s. The etching rate at 25 °C was 1 nm/s. The CTF was then rinsed in water and dried by blowing dry nitrogen on it. Thereafter, R was measured again in the set-up over the same range of θ. The measured data is presented in Fig. 3(b). Clearly, the
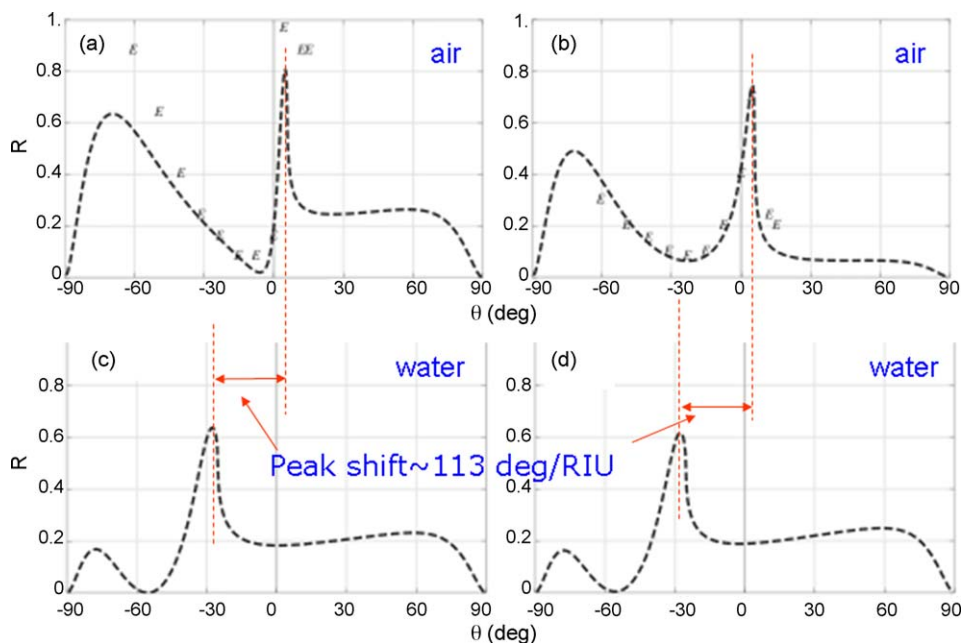
Fig. 3. Measured values of R versus θ (denoted by E), when the metal film is (a) a pre-etching Al CTF and (b) a post-etching Al CTF. The dashed lines are best fit numerical simulations obtained with (a) $p = 0.517$ and (b) $p = 0.560$ when the analyte is air. (c) and (d): Theoretical results corresponding to the same porosities as in (a) and (b), respectively but using water as analyte with refractive index of 1.33.

SPR dip is very different from that in Fig. 3(a). Numerical simulation of R and fitting to the experimental data suggests that $p = 0.56$. In other words, etching increased the porosity from 0.517 by 0.043, and the effect was captured by a widening of the SPR dip.

CTFs prepared by the oblique-angle-deposition technique are highly discontinuous when their thickness is less than 50 nm, as they are made of nanoislands but with some orientational order which builds up more and more nanowire-like as the thickness increases. [24] As SPR in the Kretschmann configuration had been previously excited only with low-porosity thin films, the possibility of its excitation using very porous metallic CTFs less than 50 nm thick was questionable. Here we have now shown both theoretically and experimentally that SPR excitation is possible on sub-50 nm thick Al CTFs with porosity ~0.5. As the porosity increases, the SPR dip widens and becomes asymmetric because of increasing scattering losses in the CTF that are due to the non-homogeneous distribution of matter therein. As the porosity increases beyond 0.75, the SPR dip almost disappears, with a vestigial peak near the onset to the TIR regime [24].

Next, numerical simulations were carried out with the assumptions that (i) the analyte is water of refractive index 1.33, and (ii) the void regions of the Al CTF are completely filled with the analyte. Fig. 3(c) and (d) shows the results for $p = 0.517$ and 0.56, the same

values of porosity as obtained from experimental data in Figs. 3(a) and (b), respectively. A comparison of the two sets of figures reveals that the SPR peak shifts by ~37.5° when the refractive index of the analyte changes by 0.33, thereby indicating a strong sensitivity of ~113°/RIU,[1] larger than the calculated sensitivity of the SPR from a nonporous ($p = 0$) Al film (~79°/RIU).

4.2. Absorption loss

The appearance of a peak at the onset of the TIR regime when the SPR broadens can also be seen when the broadening is due to absorption loss rather than scattering loss inside a thin metal film. Al and Cr, for examples, have bulk refractive indexes with high imaginary parts at 653 nm wavelength ($1.39 + 7.65i$ for Al and $3.102 + 3.334i$ for Cr); therefore, absorption loss is strong in these metals. In order to verify whether the broadening of the SPR dip can also be due to absorption loss, we both carried out experiments for dense films of Cr and simulated their SPR phenomenon as nonporous ($p = 0$) thin films of Cr. There cannot be significant scattering loss in a dense film.

Fig. 4 shows R–ϕ curves for an 8 nm-thick Cr film deposited on a glass substrate and incorporated in the
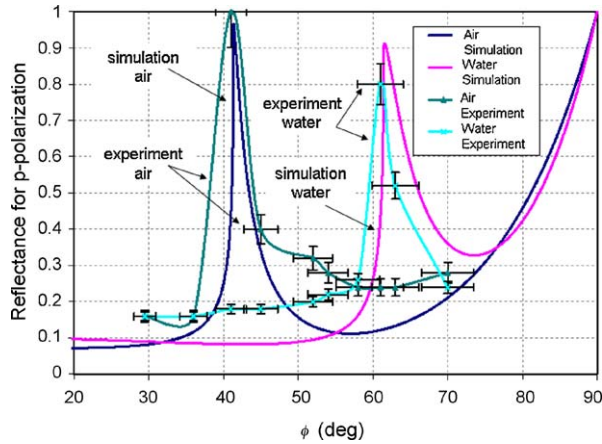
---

[1] Refractive index unit.

Fig. 4. Measured/simulated data for *p*-polarization reflectance *R* versus the angle ϕ, when the dense/nonporous (*p* = 0) metal film is 8 nm-thick and made of Cr. The curves exhibit a broad dip and a sharp and symmetric peak due to the absorption in bulk Cr. The analyte sensed is either air or water (refractive index = 1.33).

Kretschmann configuration of Fig. 2. Simulations with air and water as analytes were performed using the 2×2 Abeles matrix method. [25] For the experiment with water, a plastic tank was filled with water and glued to the glass substrate with silicone rubber. As the angle $\phi = (\pi/4) - \sin^{-1}(\sin \theta/1.51509)$ is varied, a strong peak appears followed by a deep dip in each curve. Comparison between the results for the two analytes (air and water) indicates a strong sensitivity of the angle θ to the refractive index change ($\sim 93°$/RIU) in the region set aside for occupation by an analyte.

Fig. 5 shows the intensity distribution of a diverging beam showing a peak region for *p*-polarized light which does not appear for *s*-polarized light. Hence using a CCD camera and image processing, one should be able to determine the angular peak location and use it to estimate the spatial variations of the refractive index of the analyte.

4.3. Role of porosity

Since the CTFs were made of Al, we also performed simulations for SPR from nonporous (*p* = 0) films of Al, as shown in Fig. 6. Due to absorption, a sharp and symmetric peak is obtained for nonporous Al films as thin as 4 nm; for thicker films, the SPR dip appears. A sharp and symmetric peak is obtained with a thickness of 30 nm for a CTF with ~ 0.3 porosity (calculated but not shown), while only a 4 nm thickness is required with the nonporous film. This observation should be correlated with absorption loss in a CTF ($p \sim 0.3$) being much lower than in a nonporous film (*p* = 0) of the same metal.

However, porosity also induces SPR broadening due to scattering loss inside a porous film. In order to understand how one can distinguish between the roles of porosity and intrinsic absorption in the appearance of the SPR phenomenon, we simulated the *p*-polarized reflectance from nonporous Au films, because the imaginary part of the bulk refractive index of Au ($0.1498 + 3.423i$) is almost half that of Al.

As can be seen in Fig. 7, a sharp and symmetric peak is obtained with 25 nm-thick nonporous Au film which is not very different in thickness from a 30 nm-thick, 30% porous, Al CTF. We cannot deduce from this fact that the losses in the nonporous Au film and in the Al
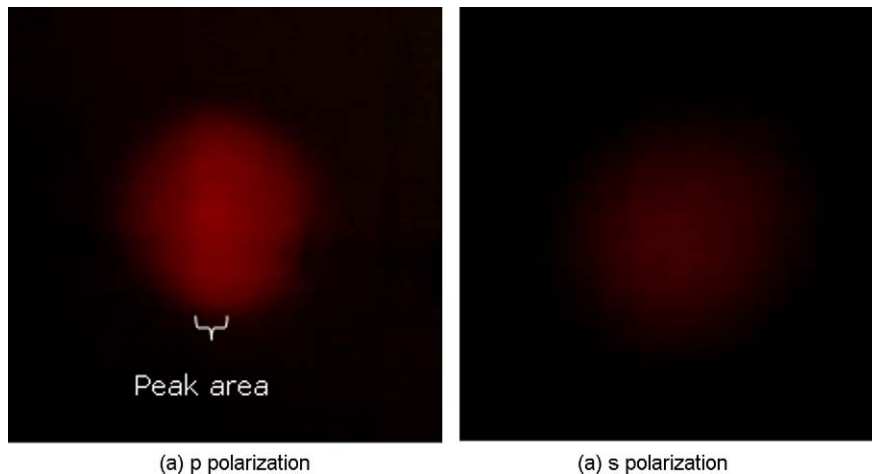

Fig. 5. Intensity distribution of the reflected diverging beam for the two polarization states: (a) *p* and (b) *s*. A peak area is clearly seen for the *p*-polarization state.
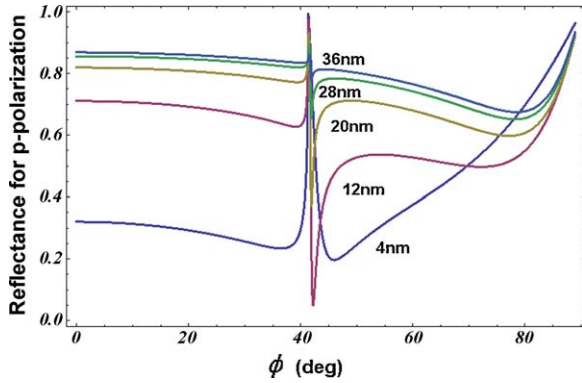
Fig. 6. Simulated data for *p*-polarization reflectance *R* versus the angle ϕ, when the metal film is nonporous Al of different thicknesses. Broad SPR dips exist for all thicknesses, and a sharp and symmetric peak is obtained for 4-nm thickness. The analyte is air.

CTF are similar because the reflection level around the remnant peak is different. Comparing now Figs. 6 and 7, we notice that the higher the loss, the lower the reflectance *R* on both sides of the peak. This is due to the fact that, both at the onset of TIR and in the excitation of the SPR, we have a surface wave which gets absorbed or scattered more, depending on the nature of the loss on the metallic side of the metal–analyte interface. If so, then we can conclude from Figs. 3 and 6 that the Al CTF is more dissipative than the nonporous Al film.

Assuming an exponentially decaying wave, we get from the reflectance near the sharp and symmetric peaks for Al films in Figs. 3 and 6 that:

$$R_{\mathrm{CTF}} = e^{-\mu_{\mathrm{CTF}}\xi_{\mathrm{CTF}}} \approx 0.1,$$
$$R_{\mathrm{nonporous}} = e^{-\mu_{\mathrm{nonporous}}\xi_{\mathrm{nonporous}}} \approx 0.2, \tag{1}$$

where μ is the attenuation coefficient – which is basically an absorption coefficient for the nonporous film,
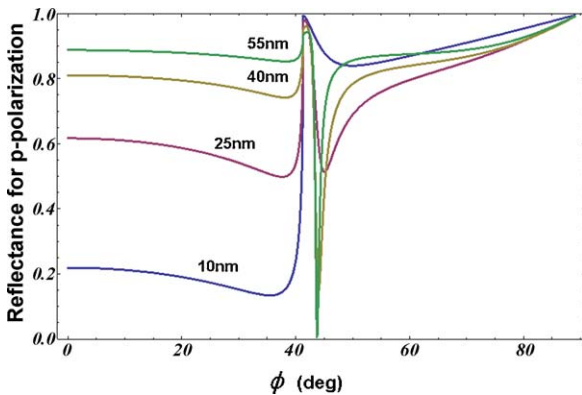

Fig. 7. Same as Fig. 6, but for dense nonporous Au films. Broad SPR dips exist for all thicknesses, and a sharp and symmetric peak is obtained for 25 nm thickness.

but includes a scattering coefficient for the CTF, i.e., $\mu_{\mathrm{CTF}} = \mu_{\mathrm{CTF\text{-}absorption}} + \mu_{\mathrm{CTF\text{-}scattering}}$ – while ξ denotes the distance traveled by the surface wave along the metal–analyte interface. Solving these equations, we obtain the following optical densities: $\mu_{\mathrm{CTF}}\xi_{\mathrm{CTF}} \approx 2.302$ and $\mu_{\mathrm{nonporous}}\xi_{\mathrm{nonporous}} \approx 1.609$. Assuming the absorption part is similar for the porous and nonporous films (i.e., $\mu_{\mathrm{CTF\text{-}absorption}}\xi_{\mathrm{CTF}} \approx \mu_{\mathrm{nonporous}}\xi_{\mathrm{nonporous}}$), we get $\mu_{\mathrm{CTF\text{-}scattering}}\xi_{\mathrm{CTF}} \approx 0.69$ which is about 43% of the absorption part and is due to the porosity of the CTF.

The imaginary parts of the bulk refractive indices (extinction coefficients) of Ag and Au are smaller by about a factor of 2 than that of Al at the wavelength of interest (653 nm). Hence, the broadening of the SPR dip is expected to be primarily induced by the disordered nanostructure (variations in the columnar dimensions and tilt angle). As can be seen in Fig. 7, it is possible to get a symmetric peak at the TIR onset when a nonporous Au film is 25 nm-thick; however, the peak height relative to the reflection level outside the peak region is 0.45 and the SPR dip is still prominent. In contrast, Fig. 6 shows a TIR peak height of 0.8 and a
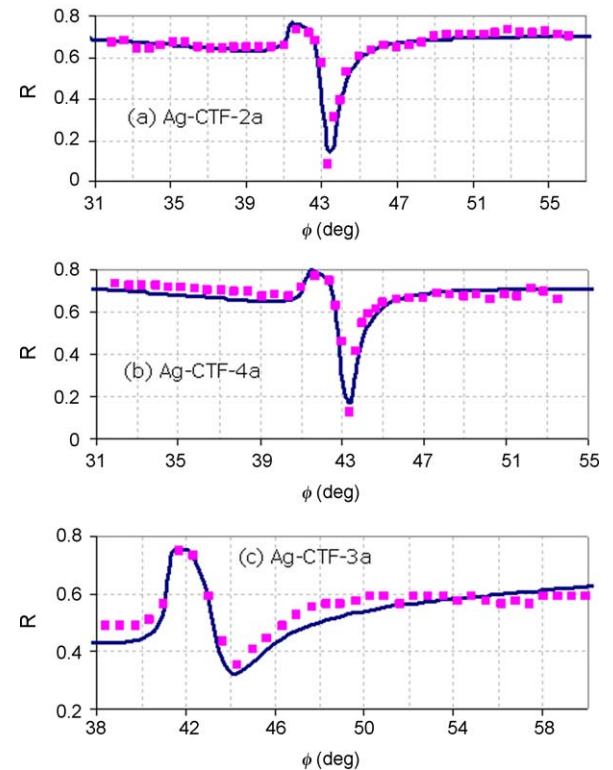

Fig. 8. *p*-polarization reflectances of Ag-CTFs in the Kretschmann configuration versus the angle ϕ. Dots are experimental data points while the curves are the theoretical fits obtained from simulations using the parameters listed in Table 1. The analyte is air.

broad SPR dip for a 4 nm-thick nonporous Al film. The differences are due to the relatively smaller extinction coefficient of bulk Ag in comparison to that of bulk Al.

4.4. Double-layer model

Several Ag- and Au-CTFs were prepared for the purpose of further investigation as these two metals are less absorptive and usually used with SPR sensors. The samples used are listed in Table 1. Figs. 8 and 9 show the p-polarization reflectance data obtained using the Kretschmann configuration, whereas the solid curves are the theoretical fits obtained using the parameters listed in Table 1. In order to get the best fits, each Ag/Au-CTF was considered as composed of two layers having different porosities, thicknesses, and ellipsoidal shape factors. This is in contrast to Al CTFs which were adequately modeled by a single layer each.

The thickness of the first layer in the double-layer models of Ag- and Au-CTFs is in the range 3–15 nm, whereas the first layer has a higher porosity than the second layer. A closer look at the cross-section SEM images in Figs. 1(c) and (e) indicates a more porous region near the substrate indeed, which is also in accord with numerous observations on CTFs of all kinds.[27,26] For the three CTFs labeled Ag-CTF-3a, Au-CTF-3a and Au-CTF-4a, the SPR dip is broad and not very pronounced, but it clearly exists. The theoretical fits show that high porosities exist in these

three CTFs. It should be noted that a multi-parameter fitting process was used and sometimes there are more than one set of parameters giving reasonable fits. The best fit was selected as the one that closely describes the true physical structure of the CTF.

4.5. Enhanced sensitivity for sensing

One of our motivations for investigating CTFs for sensing is their porous structure. The porosity increases the surface-to-volume ratio and thus the sensitivity is expected to increase. This has been demonstrated in Fig. 3 for Al-CTFa when the SPR dip turns into peak at the onset of TIR.

To investigate the sensitivity enhancement as a function of the porosity, we simulated the p-polarization reflectances of Ag-CTF-2a using the double-layer model where we kept the porosity of the 1st layer fixed and varied the porosity of the 2nd layer. In Fig. 10 the sensitivity is plotted versus the porosity of the second layer for different fixed values of the porosity of the first layer in the double-layer model. As the porosity of the second layer increases, so does the sensitivity which is enhanced by a factor of 2 for $p_2 \approx 0.3$. Similar results were obtained using the Au-CTFs in Table 1. We conclude that the use of CTFs of Au or Ag will result in enhancement of the sensitivity of SPR sensors in relation to nonporous films of the same metals. The widening of the SPR dip with increasing porosity can be
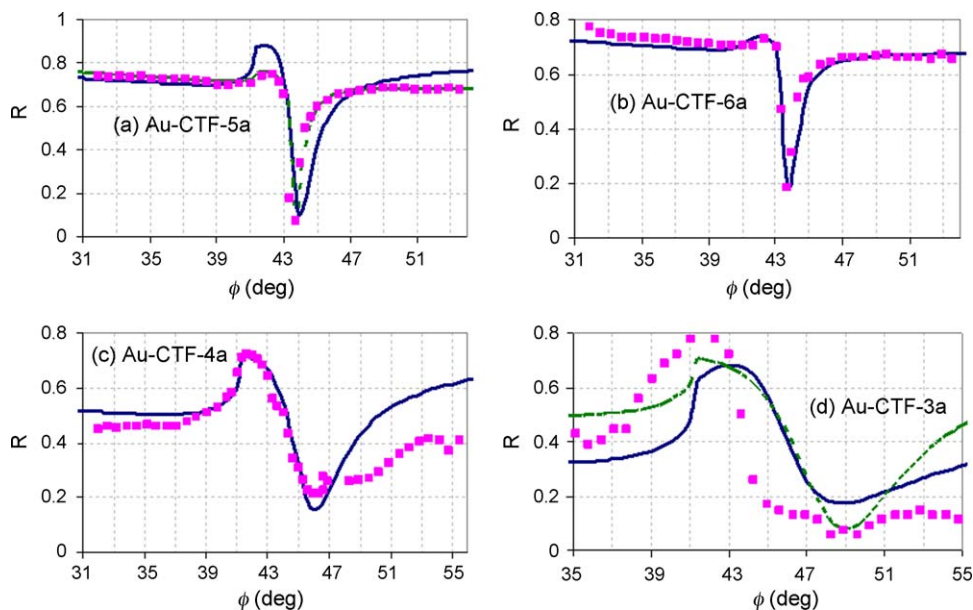

Fig. 9. p-polarization reflectances of Au-CTFs in the Kretschmann configuration versus the angle ϕ. Dots are experimental data points while the curves are theoretical fits obtained from simulations using the parameters listed in Table 1. The analyte is air. The dashed green curves in (a) and (d) correspond to different parameters (2nd set in Table 1).
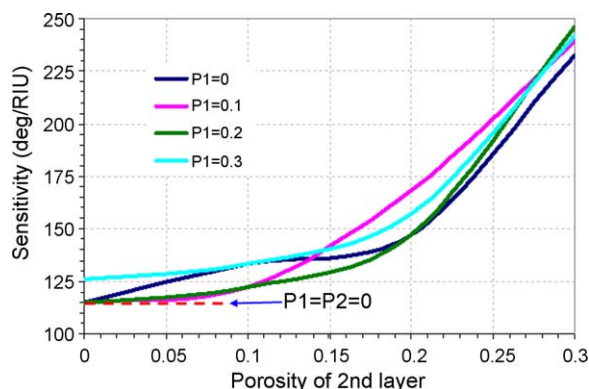
Fig. 10. Simulation results to demonstrate the sensitivity enhancement as the porosity increases. The parameters of the double-layer model of Ag-CTF-2a (Table 1) were used. Calculated sensitivity when the porosity of the (thinner) first layer is kept fixed as indicated in the legend while the porosity of the (thicker) second layer is varied from 0 to 0.3. (For interpretation of the references to color in this figure legend, the reader is referred to the web version of the article.).

overcame by using subpixelling algorithms, as was demonstrated recently. [27]

5. Concluding remarks

In the Kretschmann configuration, the excitation of SPR from porous metallic columnar thin films is possible. In The SPR dip widens as the porosity increases until it disappears, leaving behind only a peak near the onset of the TIR regime. The excitation of the SP wave at the onset of the TIR regime, combined with scattering and/or absorption losses causes the p-polarization reflectance to decrease for angles of incidence θ on the right side of the peak while the SPR excitation causes it to decrease on the left side of the peak. Under certain conditions, both sides of the peak are equally steep and the peak is then symmetric in shape. Experimental data indicates that, due to absorption loss, a very thin nonporous film exhibits a symmetric SPR peak in air as well as in water, with high sensitivity. Hence, this approach of using lossy metals with optimum thickness to obtain a narrow symmetric peak widens the possibilities for SPR sensors by making available a larger variety of materials.

Although investigated by others in the past, thin films of porous metals have not been widely used as SPR sensors because of their wide SPR dip. Our theoretical and experimental results suggest their use as sensors based on the remnant peak at the onset of the TIR regime. The use of porous metallic CTFs will facilitate the development of sensors with high sensitivity, as the ratio of surface to volume increases. For example, with

30 nm-thick Al CTFs, the sensitivity using the SPR peak mode is enhanced by a factor of about 1.5 in comparison to standard SPR sensors. For Ag- and Au-CTFs the SPR dip sensitivity increases by about a factor of 2 with 30% porosity as compared to nonporous films.

References

[1] S. Lal, S. Link, N.J. Halas, Nano-optics from sensing to waveguiding, Nat. Photonics 1 (2007) 641–648.

[2] H. Raether, Surface Plasmons on Smooth and Rough Surfaces and on Gratings, Springer, Berlin, 1988.

[3] I. Abdulhalim, M. Zourob, A. Lakhtakia, Surface plasmon resonance sensors: a mini-review, Electromagnetics 28 (2008) 214–242.

[4] P. Lecaruyer, M. Canva, J. Rolland, Metallic film optimization in a surface plasmon resonance biosensor by the extended Rouard method, Appl. Opt. 46 (2007) 2361–2369.

[5] K.L. Kelly, E. Coronado, L. Zhao, G.C. Schatz, The optical properties of metal nanoparticles: the influence of size, shape, and dielectric environment, J. Phys. Chem. B 107 (2003) 668–677.

[6] S.A. Kalele, N.R. Tiwari, S.W. Gosavi, S.K. Kulkarni, Plasmon-assisted photonics at the nanoscale, J. Nanophotonics 1 (2007) 012501.

[7] A.K. Sarychev, V.M. Shalaev, Field distribution, Anderson localization, and optical phenomena in random metal-dielectric films, in: V.A. Markel, T. George (Eds.), Optics of Nanostructured Materials, Wiley, New York, NY, USA, 2000, pp. 227–282.

[8] A. Lakhtakia, R. Messier, Sculptured Thin Films: Nanoengineered Morphology and Optics, SPIE Press, Bellingham, WA, USA, 2005.

[9] A.I. Maaroof, A. Gentle, G.B. Smith, M.B. Cortie, Bulk and surface plasmons in highly nanoporous gold films, J. Phys. D: Appl. Phys. 40 (2007) 5675–5682.

[10] F. Yang, G.W. Bradberry, J.R. Sambles, The study of the optical properties of obliquely evaporated nickel films using IR surface plasmons, Thin Solid Films 196 (1991) 35–46.

[11] M. Suzuki, W. Maekita, Y. Wada, K. Nakajima, K. Kimura, T. Fukuoka, Y. Mori, In-line aligned and bottom-up Ag nanorods for surface-enhanced Raman spectroscopy, Appl. Phys. Lett. 88 (2006) 203121.

[12] S. Shanmukh, L. Jones, J. Driskell, Y. Zhao, R. Dluhy, R.A. Tripp, Rapid and sensitive detection of respiratory virus molecular signatures using a silver nanorod array SERS substrate, Nano Lett. 6 (2006) 2630–2636.

[13] S. Ahl, P.J. Cameron, J. Liu, W. Knoll, J. Erlebacher, F. Yu, A comparative plasmonic study of nanoporous and evaporated gold films, Plasmonics 3 (2008) 13–20.

[14] I. Abdulhalim, A. Karabchevsky, C. Patzig, B. Rauschenbach, B. Fuhrmann, Comparative study of enhanced fluorescence from nano sculptured thin films, Proc. SPIE 7041 (2008) 70410G.

[15] I. Abdulhalim, A. Karabchevsky, C. Patzig, B. Rauschenbach, B. Fuhrmann, E. Eltzov, R. Marks, J. Xu, F. Zhang, A. Lakhtakia, Surface-enhanced fluorescence from metal sculptured thin films with application to biosensing in water, Appl. Phys. Lett. 94, (2009) 063206.

[16] T. Inagaki, J.P. Goudonnet, P. Royer, E.T. Arakawa, Optical properties of silver island films in the attenuated-total-reflection geometry, Appl. Opt. 25 (1986) 3635–3639.

[17] J.W. Little, T.A. Callcott, T.L. Ferrell, E.T. Arakawa, Surface-plasmon radiation from ellipsoidal silver spheroids, Phys. Rev. B 29 (1984) 1606.

[18] F. Yang, G.W. Bradberry, J.R. Sambles, Long-range surface mode supported by very thin silver films, Phys. Rev. Lett. 66 (1991) 2030–2032.

[19] A. Lakhtakia, B. Michel, W.S. Weiglhofer, The role of anisotropy in the Maxwell Garnett and Bruggeman formalisms for uniaxial particulate composite media, J. Phys. D: Appl. Phys. 30 (1997) 230–240.

[20] W.S. Weiglhofer, A. Lakhtakia, B. Michel, Maxwell Garnett and Bruggeman formalisms for a particulate composite with biani-sotropic host medium, Microw. Opt. Technol. Lett. 15 (1997) 263–266, correction: 22, 221 1999.

[21] I. Abdulhalim, A. Lakhtakia, A. Lahav, F. Zhang, J. Xu, Porosity effect on surface plasmon resonance from metallic sculptured thin films, Proc. SPIE 7041 (2008) 70410C, doi:10.1117/12.794135.

[22] J.A. Sherwin, A. Lakhtakia, I.J. Hodgkinson, On calibration of a nominal structure–property relationship model for chiral sculptured thin films by axial transmittance measurements, Opt. Commun. 209 (2002) 369–375.

[23] www.transene.com/aluminum.html.

[24] R. Messier, J.E. Yehoda, Geometry of thin-film morphology, J. Appl. Phys. 58 (1985) 3739–3746.

[25] F. Abéles, Investigations on the propagation of sinusoidal electromagnetic waves in stratified media. Application to thin films, Ann. Phys. (Paris) 5 (1950) 596–640.

[26] R. Messier, The nano-world of thin films, J. Nanophotonics 2 (2008) 021995.

[27] A. Lahav, M. Auslender, I. Abdulhalim, Sensitivity enhancement of guided wave surface plasmon resonance sensors, Opt. Lett. 33 (2008) 2539–2541.